NEUROSCIENCE
RESEARCH ARTICLE
X. Wen et al. / Neuroscience 391 (2018) 13–24

Dynamic Top-down Configuration by the Core Control System During Working Memory

Xiaotong Wen,[a] Hailing Wang,[b] Zhenghao Liu,[a] Chenghua Liu,[a] Kang Li,[a] Mingzhou Ding[c] and Xia Wu[b]*

[a] *Department of Psychology, Renmin University of China, Beijing 100872, China*

[b] *College of Information Science and Technology, Beijing Normal University, Beijing 100088, China*

[c] *The J. Crayton Pruitt Family Department of Biomedical Engineering, University of Florida, Gainesville, FL 32611, USA*

Abstract—The central executive system (CES) may be the most fundamental yet least understood component of working memory. There is an ongoing debate about which brain regions underlie the top-down regulation of CES during working memory tasks. The neural substrates and regulatory mechanisms of CES remain controversial partly because few previous studies have been focused on comprehensive activation and deactivation joint analysis on all systems involved in all working memory stages, which have shown increasing importance in depicting the neural configuration of working memory. To address these questions, we conducted a functional magnetic resonance imaging study using a comprehensive activation-deactivation-behavior joint analysis to examine the dynamics of a set of cortical systems in healthy subjects performing a modified Sternberg working memory task which was designed to push the subjects to their limit in working memory and to introduce strong demands for regulation by CES. We assessed brain activity during various working memory stages using general linear model and single trial-stage estimation, and examined the relationship between the single trial-stage activity and behavioral performance. We identified constant activation in the dorsal anterior cingulate cortex and anterior insula in all working memory stages and its relationship with performance, which indicate the CES's neural basis. We also identified dynamic configuration of multiple downstream systems in different working memory stages, which indicates the regulation mechanism of CES.

Key words: fMRI, central executive system, dorsal anterior cingulate cortex, anterior insula, top-down regulation.

INTRODUCTION

Working memory (WM) refers to a limited-capacity system that temporarily stores information and supports human thought processes by providing an interface between perception, long-term memory, and action (Baddeley, 2012). Understanding its neural mechanism is important for many applications including neuropsychology, psychiatry, development, aging, treatment of related deficits, and rehabilitation (Chacko et al., 2014; Constantinidis and Klingberg, 2016; D'Esposito and Postle, 2015; Dovis et al., 2012; Eriksson et al., 2015; Hanslmayr et al., 2012; Kofler et al., 2010; Redick et al., 2013; Stopford et al., 2012). In the WM model proposed by Baddeley and his colleagues (Baddeley, 1974; Baddeley, 2000; Baddeley and Wilson, 2002), human WM comprises a central executive system (CES), a visuospatial sketchpad, a phonological loop, and an episodic buffer. It is proposed that the CES controls the information flow to and from the slave components for temporal maintenance (Baddeley, 2012). This makes the CES the most fundamental WM component, yet many studies over the past decades have focused on single components of the model, especially the slave components (Baddeley, 2012; Eriksson, et al., 2015; Miller and Erickson, 1996; Pesaran et al., 2002). This result in the CES being the least understood component and its neural substrates being subject to debate.

There is an ongoing debate about which regions and networks underlie the top-down control of CES during WM tasks. Accumulating evidence suggests several

*Corresponding author.
E-mail address: wuxia@bnu.edu.cn (X. Wu).

Abbreviations: ACC, anterior cingulate cortex; AI, anterior insula; aPFC, anterior prefrontal cortex; BOLD, blood oxygen level-dependent; CCN, core control network; CES, central executive system; d, dorsal; dACC, dorsal anterior cingulate cortex; DLPFC, dorsal lateral prefrontal cortex; DMN, default mode network; FEF, frontal eye field; fMRI, functional magnetic resonance imaging; FPN, frontoparietal network; GLM, general linear model; IFG, inferior frontal gyrus; IPL, inferior parietal cortex; IPS, intraparietal sulcus; l, left; LOC, lateral occipital cortex; LTC, lateral temporal cortex; MNI, Montreal Neurological Institute; MPFC, middle prefrontal cortex; PCC, posterior cingulate cortex; PI, posterior insula; PMFG, posterior middle frontal gyrus; pMTC, posterior middle temporal cortex; pRO, posterior Rolandic operculum; r, right; ROI, region of interest; RT, response time; S-II, secondary somatosensory cortex; STG, superior temporal gyrus; TEO, inferior temporal cortex; v, ventral; V1, primary visual cortex; V3/V3a, visual areas 3 and 3a; WM, working memory.

https://doi.org/10.1016/j.neuroscience.2018.09.004
0306-4522/

candidate regions and networks in the prefrontal and parietal cortices that may underlie CES functions (Xu, 2017), but no consensus has yet been reached. For example, in an early opinion based on the individual WM task activation results from 6 subjects, D'Esposito et al. (1995) suggested that a set of frontal regions including the anterior cingulate cortex and the dorsal lateral prefrontal cortex (DLPFC) forms the neural basis of the CES. In later functional magnetic resonance imaging (fMRI) studies, Osaka et al. (2007) and Osaka et al. (2004) showed that subjects with longer memory spans exhibit stronger activation in the ACC and inferior frontal gyrus (IFG) and accordingly hypothesized that those regions may be associated with the working attention control of the CES. However, it is proposed that a set of dorsal frontoparietal areas comprising the bilateral frontal eye field, superior parietal gyrus, and intraparietal sulcus are essential for WM due to the areas' robust activation during WM tasks, forming a so-called WM network (Courtney et al., 1997; Curtis, 2006; Leung et al., 2004; Merrikhi et al., 2017; Pessoa et al., 2002; Wu et al., 2018; Xu et al., 2014). These regions are also activated when top-down attention control is implemented and are thus believed to form a network for goal-directed attention control (Corbetta et al., 2008), though whether they form a "WM network" or an "attention network" is a long-debated issue. Some researchers have proposed that this frontoparietal network (FPN) stores task information during both WM and attention tasks (Corbetta et al., 2002). A recently proposed alternative opinion suggests that the so-called central executive network for maintaining and manipulating information in WM may be anchored in the DLPFC and posterior parietal cortex (Bressler and Menon, 2010; Menon, 2015). There is also an emerging opinion that many cognitive processes including WM rely on a shared neural mechanism for central executive control (D'Esposito and Postle, 2015; Harding et al., 2016); namely, a core control network (CCN) that supports the dynamic and effective production of diverse behaviors (Corbetta, et al., 2008). The CCN's specific components remain unclear, but some studies indicate that they may include the DLPFC, dorsal ACC (dACC), anterior insula (AI), inferior frontal junction, and posterior parietal cortex (Cole and Schneider, 2007). However, Dosenbach et al. (2006) hypothesized that a CCN comprising areas commonly activated during highly demanding tasks, which mainly includes the dACC and AI, may provide top-down regulation of downstream systems to guarantee performance in various goal-directed tasks, though whether and how this core regulation system applies to WM remains unclear. Controversy on which of the frontoparietal network and the ACC-AI network plays the core role in WM also remains. A recent magnetoencephalography study suggested that the former is responsible for top-down modulation while the latter plays a more downstream role in WM (Wallis et al., 2015), which is in conflict with some previously proposed models (Dosenbach, et al., 2006).

In summary, the neural basis of the CES, its relation to the CCN, and its functions in relation to WM remain elusive. The limited understanding of its neural substrates may be associated with the limitations of previous studies, which for decades have been focused on brain activation during various WM conditions (Cohen et al., 2014; Rypma et al., 1999), with fewer systematically examining WM activation, deactivation, and the activation-deactivation relationship. However, several recent studies have demonstrated the importance of deactivation in WM (Anticevic et al., 2013; Anticevic et al., 2010; Piccoli et al., 2015), indicating that the hypotheses and network models mentioned above, which only been considered within regions activated during WM, may hinder the identification of regions associated with the CES and their mechanisms for regulating the slave components. According to the literature, the CCN shows robust activation in many cognitively demanding tasks including WM, and was proposed to regulate the other downstream systems according to different task sets. We hypothesized that during WM, the core regions of the CCN may function as the neural basis of the CES, regulating the slave systems according to demands of different WM stages. A comprehensive analysis of the spatial and temporal pattern of both activation and deactivation may help to identify the neural basis of the CES and scrutinize its regulation to other systems.

To address these questions and test our hypothesis, we conducted an fMRI study using a general linear model (GLM) and single trial-stage analysis to examine brain activation and deactivation in healthy subjects performing a modified Sternberg WM task with an event-related design. The task was designed to push the subjects to their limit in WM and to introduce significant stage-dependent activation/deactivation of multiple subsystems which demands for dynamic regulation by CES. We measured blood oxygen level-dependent signals as a proxy for brain activity during the encoding, maintenance, and probe stages of WM and investigated the relationship between stage-dependent brain activity and behavioral performance.

EXPERIMENTAL PROCEDURES

Participants

Nineteen young healthy right-handed individuals (11 men, mean age: 25.26 years, standard deviation: 2.79 years) with normal or corrected-to-normal vision were recruited. All participants were students from Beijing Normal University. Each subject filled a screening form to report psychiatric history and drug use. None had a history of psychiatric illness or recreational drug usage, or was currently taking medications that could affect the central neural system. This study was approved by Beijing Normal University's Institutional Review Board and conducted in accordance with the principles of the Declaration of Helsinki. All participants gave written informed consent. Each participant received a compensation of 100 Chinese Yuan. All participants participated an out-scanner task training session in a pre-scanning visit, were fully informed about the scanning environment, safety rules, and scanning procedure during their pre-scan visit. One woman quit the experiment halfway, so her data were excluded from analysis.

Modified Sternberg's WM task

The Sternberg WM Task is an established test of WM performance and tool for investigating the WM process (Peterburs et al., 2016; Reed et al., 2017). Each trial was divided into a 2-s baseline stage with a fixation point in the middle of the screen; a 3-s encoding stage during which a load condition of 0, 3, 5, or 9 letters was displayed; a 7-s maintenance stage with fixation; and a 300-ms probe stage during which a letter was shown in the middle of the screen. The inter-trail interval randomly varied between 5 and 7 s (Fig. 1A). If letters were presented during the encoding stage, then the subjects were asked to memorize the letters, remember them during the maintenance stage, and indicate as quickly as possible whether the letter displayed in the probe stage matched any of the memorized letters by pressing the "L" or "R" key for a match or mismatch, respectively. Capital letters were randomly selected from the alphabet, excluding L or R. Hash tags ("#") were used in place of unoccupied letter spaces (Fig. 1A). If no letters were presented during the encoding stage, then "L" or "R" was presented during the probe stage, and the subjects were asked to press the corresponding key as quickly as possible. The number of the letters to remember in the highest load condition was setting to 9 to increase the difficulty of the task and push the subjects to challenge their limit and to introduce significant stage-dependent activation/deactivation of multiple subsystems which demands for dynamic regulation by CES. The whole task was divided evenly into 3 task runs. The total number of the trials was 180. Data of the participants who had the percentage of correct-response trials higher than 70% were accepted for further analysis.

MRI data acquisition and preprocessing

All MRI data were acquired using a 3-tesla Magnetom Trio whole-body MRI system (Siemens, Munich, Germany) at the Beijing Normal University MRI Center. Functional scanning was performed using a T2*-weighted echo-planar imaging sequence (field of view = 200 mm × 200 mm, echo time = 30 ms; repetition time = 2 s; flip angle = 90°; axial slices per volume = 33; matrix size = 64 × 64; slice thickness = 3.5 mm; voxel size is 3.13 mm × 3.13 mm × 3.5 mm). For each task run, 600 whole-brain volumes were recorded. High-resolution anatomic images were acquired with a T1-weighted 144 slice MPRAGE sequence (repetition time, 2530 ms; echo time, 3.39 ms; flip angle, 7°; inversion time, 1100 ms; voxel size, 1 mm × 1.33 mm × 1 mm). The subjects were informed of the importance of keeping their heads still in the scanner, and head movement was strictly controlled with a set of memory foam adapters.

We used SPM8 software (http://www.fil.ion.ucl.ac.uk/spm/software/spm8/) for preprocessing including temporal processing (slice timing), motion correction, anatomical coregistration, normalization to Montreal Neurological Institute (MNI) space, structure image resampling to 1 mm × 1 mm × 1 mm per voxel, functional image resampling to 3 mm × 3 mm × 3 mm per voxel, and spatial smoothing with an 8-mm full-width at half-maximum Gaussian core.

GLM analysis and region of interest selection

To examine dynamic brain activation patterns in the WM task and determine the ROIs for further analysis, we conducted a GLM analysis in SPM8. For the first-level analysis, we used a high-pass filter with a cutoff frequency of 1/128 Hz. The model included 15 BOLD predictors for trial conditions and 6 head motion parameters generated in the realignment procedure. The first 12 predictors corresponded to the combination of the 3 WM stages (encode, maintain, and probe) and the 4 load conditions (0, 3, 5, or 9 letters) from correct-response trials. The next 3 predictors corresponded to the 3 WM stages from wrong-response trials. The BOLD predictors were generated by specifying the onset and duration of each event under each combination and a canonical hemodynamic response function provided by SPM8. Individual activation maps were generated by contrasting the 3-, 5-, and 9-letter load conditions against the 0-letter load condition, while individual deactivation maps were generated by contrasting the 0-letter load condition against the 3-, 5-, and 9-letter load conditions. For second-level random-effect analyses, we applied 1-sample t-tests to the individual activation/deactivation contrast maps to generate group activation/deactivation maps (T-maps).

Because the global strength of activation/deactivation varied strongly between WM stages, we used an adaptive approach to objectively define the significance

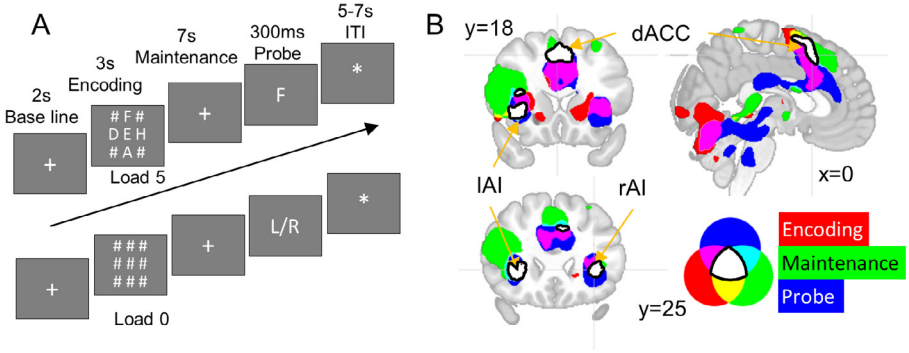

Fig. 1. A: Experimental paradigm. Under the 3-, 5-, and 9-letter load conditions, subjects were instructed to memorize the letters presented during encoding stage and then quickly indicate whether the letter displayed during the probe stage matched any of the memorized letters by pressing the "L" or "R" key for a match or a mismatch, respectively. Under the 0-letter load condition, no letter was presented during the encoding stage, and subjects were instructed to press the "L" or "R" key as soon as the corresponding letter was presented. B: The overlapped activation maps for the encoding, maintenance, and probe stages highlighted 3 core regions (white) including the dACC, left AI, and right AI that were consistently activated in all 3 working memory stages. Abbreviations: AI, anterior insula; dACC, dorsal anterior cingulate cortex; l, left; r, right.

thresholds for extracting the relatively strong activation and deactivation in different WM stages. Specifically, we sorted the in-brain voxels according to their t-values and then defined the top and bottom deciles of voxels as being strongly activated and strongly deactivated, respectively. We then superimposed T-maps of these voxels for each task stage onto a spatially normalized high-resolution MNI T1 template (Collins et al., 1994) (Fig. 1B). Regions that exhibited local maximal activation/deactivation in these T-maps were selected as ROIs for BOLD signal analyses.

Single-trial BOLD estimation

We performed single-trial BOLD estimation to examine the dynamic characteristics of ROI BOLD responses during different WM stages and under different load conditions. For each subject, ROI BOLD percentage changes were extracted and calculated from the smoothed and normalized images.

Because event onsets in the task could fall into gaps between sampling points, we tried to better fit the data to events' onsets by up-sampling the BOLD percentage change signals to a 10-Hz sampling rate and 100-ms repetition time using cubic spline interpolation. The interpolated signals for correct-responses' trials were then epoched into single-trial periods based on task onsets and durations. The epochs were then classified by load conditions. Each single-trial period was decomposed into 3 components representing activity during the encoding, maintenance, and probe stages using regressors generated by convolving the trial events with the canonical hemodynamic response function. The 0-letter load condition was defined as the baseline, and we estimated the beta value and fitted BOLD response for the contrast of 3-, 5-, and 9-letter loads against the baseline during each WM stage in each trial. We then averaged these single-trial BOLD responses for each WM stage across all trials to yield estimated mean stage-specific BOLD responses under each load condition. Finally, we averaged these mean responses across all subjects to yield group mean responses.

Correlating brain activity with behavioral performance

We explored the behavioral significance of the BOLD responses by examining whether those measured in the encoding and maintenance stages predicted behavioral performance in the probe stage. We performed correlation analysis between single-trial regional BOLD signals and response times (RTs) at the subject and group levels. This correlation analysis was designed to adapt to the variable number of correct-response trials across subjects and conditions by converting correct-response trial RTs into z-scores and then sorting and stacking the correct-response trials by those z-scores. Specifically, for a certain condition, let X_i be the number of the correct-response trials of the i_{th} participant. Because X_i might vary across participants, we stack the trials according to RT into N levels from fast to slow, where N was the same for all participants so that we could average the data (neural data or RT) across participants within each level and perform the neurobehavioral correlation analysis on a group level. To do this, we sorted the trials according to an ascending order of RT. Then each stack was centered by one of the N milestones evenly distributed along the sorted list and included M neighboring trials (M was even, M/2 on each side). The index of the j_{th} "milestone" trial for the i_{th} participant, the I_{ij}, was determined using the rounding of $M/2 + 1 + [(j-1)(X_i - M)/(N-1)]$, where $(X_i - M)/(N-1)$ was the step length between each "milestone". A similar correlation strategy was used in our previous research to correlate neural data with behavioral performance (Wen et al., 2012; Wen et al., 2013).

In the current study, we specified 25 "milestone trials" evenly distributed along the list of the sorted correct trials and combined each milestone trial and its neighboring 4 trials (2 on each side) into 1 level. We designated the group with the shortest RTs as level 1 and the group with the longest RTs as level 25. The RT z-scores and single-trial BOLD response beta values were averaged in each level. We then averaged the results for the 3-, 5-, and 9-letter load conditions for subsequent analysis. This sorting and grouping process made group analyses possible by scaling each individual's behavioral performance to a unified space despite the variable number of correct-response trials and the performance differences across subjects and conditions. We then performed group correlation analysis by averaged mean beta values across subjects for each ROI and WM stage. We used Spearman's ranked partial correlations to examine the relationship between RTs in probe stage and BOLD responses during encoding or maintenance stage while using those during other stages as control variables.

RESULTS

Behavioral performance summary

Eighteen subjects completed the experiment according to instructions. The average RT was 613.7 ± 61.6 ms for the 0-letter load, 762.8 ± 85.0 ms for the 3-letter load, 886.6 ± 94.0 ms for the 5-letter load, and 1013.3 ± 112.8 ms for the 9-letter load. The average correct-response rate was 92.1 ± 1.9% for the 0-letter load, 89.0 ± 1.5% for the 3-letter load, 91.6 ± 2.0% for the 5-letter load, and 70.0 ± 3.4% for the 9-letter load. All those subjects had an overall correct-response rate higher than 70% and their data of correct trials were included in further analysis.

A CCN constantly activated in all stages

To identify the core regions involved in all 3 WM stages, we examined the overlapping regions in the stage-specific activation maps. The minimum T-values that met our strong activation threshold were 5.68, 1.12, and 1.96 for the encoding, maintenance, and probe stages,

respectively. We found that the strongly activated regions in the different stages' T-maps overlapped in a network that included the dACC, right AI, and left AI (Fig. 1B, white region; MNI centers: 0 18 50, 36 25 8, and −34 19 3, respectively). These overlapping regions are anatomically consistent with the CCN proposed by Dosenbach, et al. (2006).

Dynamic activation and deactivation patterns in different WM stages

We found that activation in the encoding stage was intense, widespread, slightly left-lateralized, and included several networks and regions ($p < 0.00005$, false discovery rate-corrected). We observed activation of the CCN, which comprises the right dACC and bilateral AIs (Dosenbach et al., 2007); the FPN, which comprises the bilateral frontal eye fields and intraparietal sulcus (Corbetta, et al., 2008); phonological regions, which comprise the left posterior middle frontal gyrus and left inferior temporal cortex (Aboitiz et al., 2010; Chein et al., 2003; Glezer et al., 2016; Hickok and Poeppel, 2007; Logie, 2003); and various visual areas, which comprise the primary visual cortex and lateral occipital cortex. Deactivation, however, was much weaker. When applying a looser threshold ($p < 0.001$, uncorrected), we observed deactivation in the default mode network (DMN), the secondary somatosensory cortex (S-II), and the left superior temporal gyrus of the auditory pathway. The deactivated DMN areas included the posterior cingulate cortex, bilateral inferior parietal cortices, and bilateral temporal cortices. The deactivated S-II areas included the right posterior Rolandic operculum and bilateral posterior insula.

Compared to the encoding stage activation, the maintenance stage activation was weaker but more focused, while deactivation was stronger and more widespread. Activation could be observed in the dACC, left IFG, and left posterior middle temporal gyrus at $p < 0.002$ (uncorrected). The latter 2 areas were also proposed to be the phonological network's essential components (Aboitiz, et al., 2010; Chein, et al., 2003; Glezer, et al., 2016; Hickok and Poeppel, 2007). However, strong deactivation was observed in multiple classical DMN regions; ventral and dorsal visual pathways including the bilateral lateral occipital cortex, left inferior temporal cortex, and visual areas 3 and 3a; and S-II regions including the posterior Rolandic operculum and posterior insula ($p < 0.001$, false discovery rate-corrected). During the probe stage, the dACC and bilateral AIs were activated ($p < 0.002$, uncorrected), and deactivation was weak.

These activated and deactivated regions were chosen as ROIs for the following analysis (Table 1). The 3 stages' overall activation patterns are summarized in Fig. 2A.

We subsequently examined functional differences between the CCN and other functional networks by listing the ROIs according to the canonical functional networks (systems) that they belong to. We found that the CCN was the only system that was consistently activated in all 3 stages (Fig. 2B). The FPN was strongly activated only in the encoding stage, while the phonological network was strongly activated in the encoding and maintenance stages. The visual pathways were activated in the encoding stage but strongly deactivated in the maintenance stage. The DMN regions, however, were consistently deactivated in all 3 stages. The S-II and auditory cortex were deactivated in the encoding and maintenance stages.

$C+$ denotes core regions that were consistently activated during all 3 stages. $E+/-$, $M+/-$, and $P+/-$ denote activation and deactivation during the encoding, maintenance, and probe stages, respectively. *False discovery rate-corrected (all others were uncorrected). Abbreviations: AI, anterior insular cortex; aPFC, anterior prefrontal cortex; CCN, core control network; dACC, dorsal anterior cingulate cortex; d, dorsal; DMN, default mode network; FEF, frontal eye field; FPN, frontoparietal network; IFG, inferior frontal gyrus; IPL, inferior parietal cortex; IPS, intraparietal sulcus; l, left; LOC, lateral occipital cortex; LTC, lateral temporal cortex; MPFC, middle prefrontal cortex; MNI, Montreal Neurological Institute; PCC, posterior cingulate cortex; PI, posterior insula; PMFG, posterior middle frontal gyrus; pMTC, posterior middle temporal cortex; pRO, posterior Rolandic operculum; r, right; S-II, secondary somatosensory cortex; STG, superior temporal gyrus; TEO, inferior temporal cortex; v, ventral; V1, primary visual cortex; V3/V3a, visual areas 3 and 3a.

BOLD responses in different WM stages

For each ROI, we plotted the estimated BOLD responses averaged across trials for each load condition (Fig. 3). We found that the CCN regions, namely the dACC and AI, exhibited stronger activation under greater load conditions in all 3 WM stages. However, the FPN regions exhibited stronger encoding stage activation. The left IFG/Broca's area exhibited stronger activation in the maintenance stage, while the visual cortices, such as visual area 2, exhibited deactivation in that stage. The auditory cortex, DMN regions, and S-II regions such as the posterior insula exhibited deactivation in all 3 stages under greater load conditions.

Brain activity predicts behavioral performance

We examined whether the BOLD responses in the encoding and maintenance stages could predict behavioral performance in the probe stage. We observed significant correlations between BOLD responses and RTs ($p < 0.05$; Fig. 4). Most encoding stage correlations in the CCN were negative, indicating that greater encoding stage BOLD responses in those regions may predict faster recall in the probe stage. However, most of the detected correlations in the DMN, S-II, auditory cortex, and some visual areas were positive. Given that those regions were deactivated in the encoding stage, this indicates that stronger deactivation may correspond to faster recall. In the maintenance stage, most of the detected correlations in the DMN and S-II were positive. Only the phonological regions showed more negative correlations than positive

Table 1. Regions of local maximal activation and deactivation in different WM stages

Condition	Network	ROI	T-value	*p*-value	MNI coordinates (mm)		
					x	y	z
Co-activation	CCN	dACC (C+)			0	18	50
		rAI (C+)			36	25	8
		lAI (C+)			−34	19	3
Encode activation	CCN	ldACC (E+)	9.6	<0.00005*	−6	23	28
		rdACC (E+)	9.5	<0.00005*	6	11	55
		rAI (E+)	8.52	<0.00005*	36	17	7
		lAI (E+)	7.85	<0.00005*	–33	20	7
	FPN	rFEF (E+)	7.73	<0.00005*	27	2	64
		lFEF (E+)	10.74	<0.00005*	−27	−4	64
		rIPS (E+)	11.57	<0.00005*	24	−64	55
		rIPS2 (E+)	10.81	<0.00005*	21	−76	58
		lIPS (E+)	9.6	<0.00005*	−30	−67	52
	Visual	rV1 (E+)	12.56	<0.00005*	15	−82	−11
		lLOC (E+)	12.28	<0.00005*	−39	−79	−5
	Phonological	lPMFG (E+)	9.28	<0.00005*	−48	2	49
		lTEO (E+)	11.45	<0.00005*	−45	−67	−5
Encode deactivation	DMN	lIPL (E−)	−6.08	<0.001	−45	−82	31
		rIPL (E−)	−4.7	<0.001	54	−67	28
		lLTC (E−)	−6.08	<0.001	−63	−13	−11
		rLTC (E−)	−5.25	<0.001	51	5	−14
		PCC (E−)	−5.24	<0.001	−9	−49	40
	S-II	rpRO (E−)	−4.56	<0.001	42	−28	22
		rPI (E−)	−4.44	<0.001	42	−10	4
		lPI (E−)	−4.19	<0.001	−45	−13	4
	Auditory	lSTG (E−)	−5.35	<0.001	−42	–22	7
Maintenance activation	Phonological	lpMTC (M+)	6.83	<0.002	−39	−52	4
		lIFG (M+)	6.1	<0.002	−51	23	25
	CCN	rdACC (M+)	3.49	<0.002	9	32	40
Maintenance deactivation	DMN	laPFC (M−)	−9.2	<0.001*	−18	47	49
		rdMPFC (M−)	−10.17	<0.001*	6	65	13
		ldMPFC (M−)	−8.69	<0.001*	−6	56	13
		vMPFC (M−)	−7.4	<0.001*	0	26	−8
		PCC (M−)	−5.89	<0.001*	−6	−64	28
	Visual	rLOC(M−)	−9.24	<0.001*	36	−85	1
		lLOC (M−)	−8.35	<0.001*	−30	−94	4
		lTEO (M−)	−7.83	<0.001*	−36	−67	−11
		rV3/V3a (M−)	−8.3	<0.001*	30	−88	25
	S-II	rpRO(M−)	−7.03	<0.001*	57	−1	16
		rPI (M−)	−8.85	<0.001*	45	−13	−5
		lPI (M−)	−7.07	<0.001*	−36	−4	−11
Probe activation	CCN	rdACC (P+)	4.13	<0.001	−6	29	28
		rAI (P+)	5.21	<0.001	33	32	7
		lAI (P+)	5.41	<0.001	−30	32	10

correlations when combining the encoding and maintenance stages.

DISCUSSION

In this study, we investigated dynamic brain activation/deactivation configurations and their behavioral significance in a WM task. Our examination of the spatial distribution and strength of BOLD responses in different WM stages revealed consistent activation in the dACC and AI, the core regions of the so-called CCN, as well as dynamic activation and deactivation according to stage-specific WM requirements in other functional networks, such as the FPN, phonological network, visual pathways, auditory cortex, S-II, and DMN. Our results indicated that CCN is the neural basis of the CES which provides top-down regulation in Baddeley's WM model in WM and also showed how the slave components are regulated (Fig. 5).

Consistent dACC-AI network activation indicates a WM control center

Our observation that the dACC and AI were consistently activated in all 3 WM stages (Fig. 5) is consistent with previous reports that these regions may play important roles in top-down regulation of numerous goal-directed tasks including attention, WM, and task switching (Dosenbach, et al., 2006; Shenhav et al., 2016; Wen et al., 2013) and that damage to these regions may cause various cognitive deficits in tasks requiring top-down regulation (Bonnelle et al., 2012). Imaging studies that imple-

mented multiple task activation pattern analyses showed that these regions are robustly activated in many highly demanding tasks, including visual search, motor timing, stimulus matching, and speech generation, while other networks such as the FPN and language areas may be differentially activated according to specific tasks (Dosenbach, et al., 2006). Dosenbach, et al. (2007) accordingly proposed that they form a CCN that regulates downstream systems in such tasks. We further observed sustained CCN activation across different conditions in a WM task, which indicates that the CCN may underlie sustained top-down regulation to slave components of WM (Fig. 5).

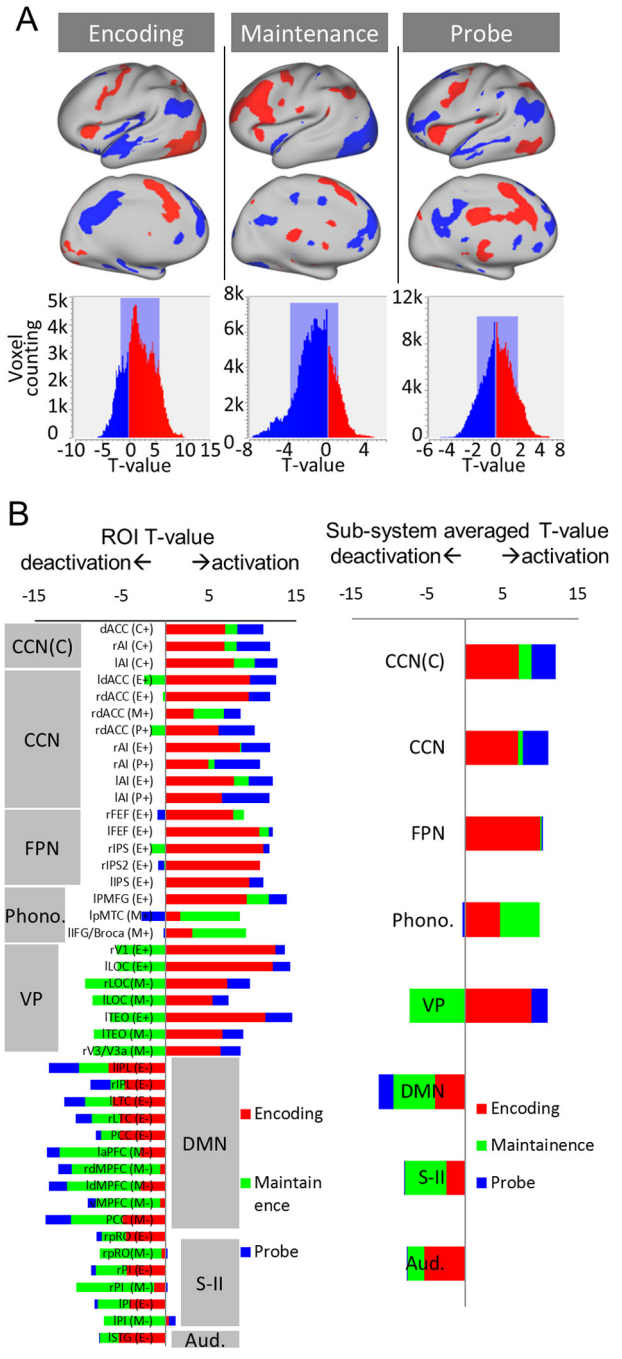

Fig. 2. A: Activation during the 3 WM stages. Voxels with T-values in the top 10% were considered strongly activated (red), while those in the bottom 10% were considered strongly deactivated (blue). The histograms summarize the activated and deactivated voxels projected onto a brain surface template. Voxels outside the shaded rectangle were considered strongly activated or strongly deactivated according to the threshold above. Note that in the encoding stage, activation was stronger and more widespread than deactivation was, while the reverse was true in the maintenance stage. B: Activation of various regions and systems in different WM stages. Left panel: Activation or deactivation of each ROI. *C+* denotes core regions that were consistently activated in all 3 stages (see Fig. 1A). *E+/−*, *M+/−*, and *P+/−* denote activation and deactivation during the encoding, maintenance, and probe stages, respectively. Right panel: Summary of the system-wide activations by averaging within each subsystem. *CCN(C)* denotes summaries of the 3 consistently activated core regions. *CCN* denotes summaries of all CCN ROIs. Abbreviations: AI, anterior insular cortex; aPFC, anterior prefrontal cortex; CCN, core control network; d, dorsal; dACC, dorsal anterior cingulate cortex; DMN, default mode network; FEF, frontal eye field; FPN, frontoparietal network; IFG, inferior frontal gyrus; IPL, inferior parietal cortex; IPS, intraparietal sulcus; l, left; LOC, lateral occipital cortex; LTC, lateral temporal cortex; MPFC, middle prefrontal cortex; MNI, Montreal Neurological Institute; PCC, posterior cingulate cortex; PI, posterior insula; PMFG, posterior middle frontal gyrus; pMTC, posterior middle temporal cortex; pRO, posterior Rolandic operculum; r, right; ROI, region of interest; S-II, secondary somatosensory cortex; STG, superior temporal gyrus; TEO, inferior temporal cortex; v, ventral; V1, primary visual cortex; V3/V3a, visual areas 3 and 3a; WM, working memory.

The functional role of the dACC and AI requires further elucidation. Some researchers have suggested that the dACC plays a central role in maintaining task control and is more prominent than the AI in top-down controlling other systems during tasks (Shenhav, et al., 2016; Wen, et al., 2013). Other studies suggest that the AI may be an important station linking the CCN with other networks and relaying top-down signals to regulate their activities (Cai et al., 2016; Menon and Uddin, 2010). As for the non-CCN systems, it seems that their activation or deactivation in the current WM task depends on WM stages and conditions.

Sustained DMN deactivation versus sustained CCN activation

In our experiment, the DMN was consistently deactivated in the encoding and maintenance stages (Fig. 5). The DMN is considered an internal interference source (Buckner et al., 2008; Elton and Wei, 2015; Wen, et al., 2013). To perform the WM task successfully, the subjects had to suppress internal interference such as mind wandering and free thinking. In the encoding and maintenance stages, most detected correlations between DMN BOLD responses and probe stage RTs were positive, such that successful DMN suppression predicted quicker task performance. Given that the CCN was the only consistently activated system while the DMN was consistently deactivated, top-down control over the DMN might come from the CCN (Fig. 5). This may explain why disrupted CCN integrity predicts attenuated DMN deactivation and impaired task performance in patients with traumatic brain injuries (Bonnelle, et al., 2012; Jilka et al., 2014). It is also consistent with our previous atten-

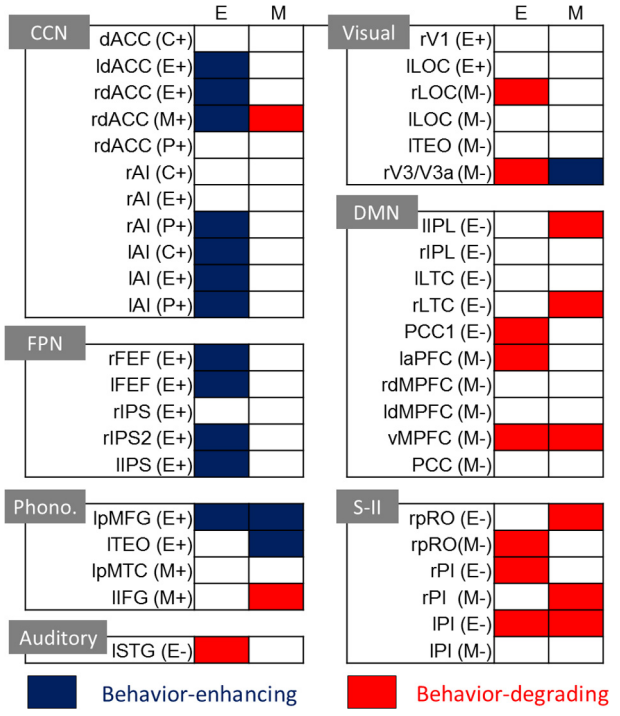

Fig. 3. Estimated mean BOLD responses of some example ROIs. Blue, green, and red refer to the 9-, 5-, and 3-letter load conditions, respectively. Thin solid lines, thin dashed lines, and dash-dot lines refer to responses in the encoding, maintenance, and probe stages, respectively. Thick lines refer to the sum of responses for all 3 stages. *C* denotes core regions that were consistently activated in all 3 stages (see Fig. 1A). *E*+/− and *M*+/− denote activation and deactivation during the encoding and maintenance stages, respectively. Abbreviations: AI, anterior insula; BOLD, blood oxygen level-dependent; dACC, dorsal anterior cingulate cortex; IFG, inferior frontal gyrus; IPS, intraparietal sulcus; l, left; LOC, lateral occipital cortex; MPFC, middle prefrontal cortex; PCC, posterior cingulate cortex; pRO, posterior Rolandic operculum; ROI, region of interest; STG, superior temporal gyrus.

tion study (Wen, et al., 2013) that found sustained CCN activation and DMN deactivation throughout the task blocks. Causal influence analysis in that study also indicated that the CCN may exert top-down DMN regulation to improve performance, while internal interference from the DMN may disturb CCN task control and degrade performance.

Sensory input-related regional activity is regulated according to WM demands

Sensory input systems were activated or deactivated according to WM task stages. For example, during the encoding stage we saw activation of the visual cortices but deactivation of the somatosensory and auditory cortices (Fig. 2). This indicates that the visual presentation of verbal stimuli caused selective attention that enhanced visual pathway processing while depressing activity in other sensory input pathways. The correlations between behavioral performance and encoding stage activation in these areas were consistent with the activation/deactivation results, such that stronger S-II and auditory cortex deactivation in the

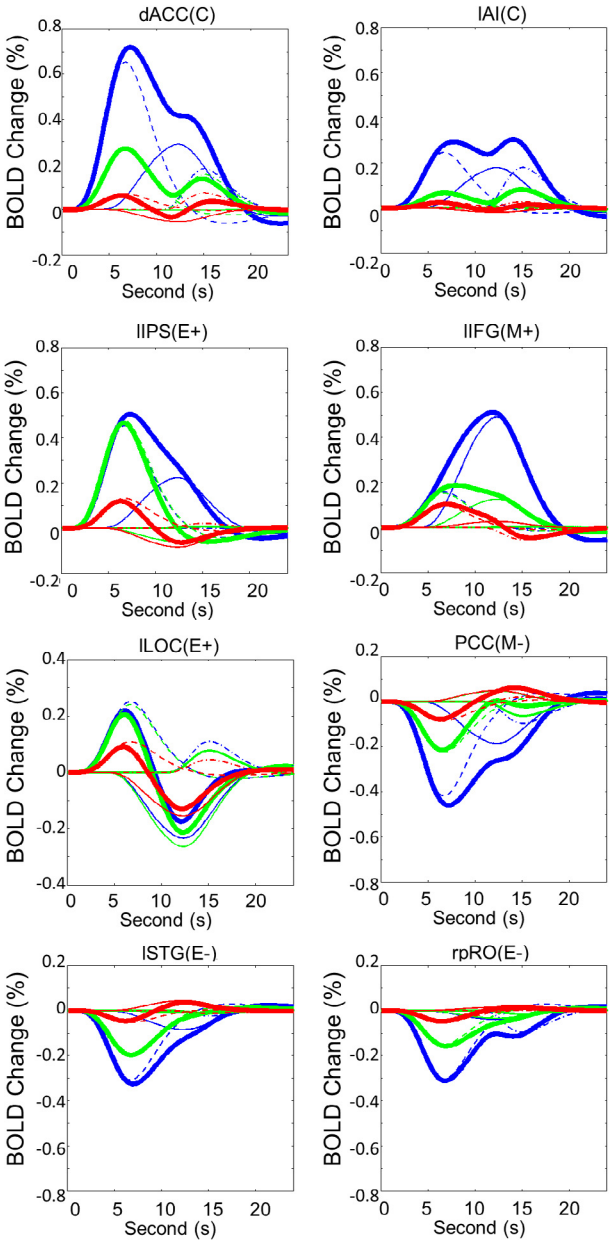

Fig. 4. Predicting behavioral performance in the probe stage from ROI-specific BOLD responses in the encoding and maintenance stages. Red and blue denote significant positive and negative correlations, respectively, between BOLD responses and RTs. Abbreviations: AI, anterior insula; aPFC, anterior prefrontal cortex; BOLD, blood oxygen level-dependent; CCN, core control network; d, dorsal; dACC, dorsal anterior cingulate cortex; FEF, frontal eye field; IFG, inferior frontal gyrus; IPL, inferior parietal cortex; IPS, intraparietal sulcus; l, left; LOC, lateral occipital cortex; LTC, lateral temporal cortex; PCC, posterior cingulate cortex; PI, posterior insula; pMFG, posterior middle frontal gyrus; pRO, posterior Rolandic operculum; r, right; ROI, region of interest; RT, response time; STG, superior temporal gyrus; TEO, inferior temporal cortex; v, ventral; V1, primary visual cortex; V3/V3a, visual areas 3 and 3a.

encoding stage predicted faster probe stage responses (Fig. 4), indicating that the suppression of task-irrelevant inputs during the encoding stage improves WM performance.

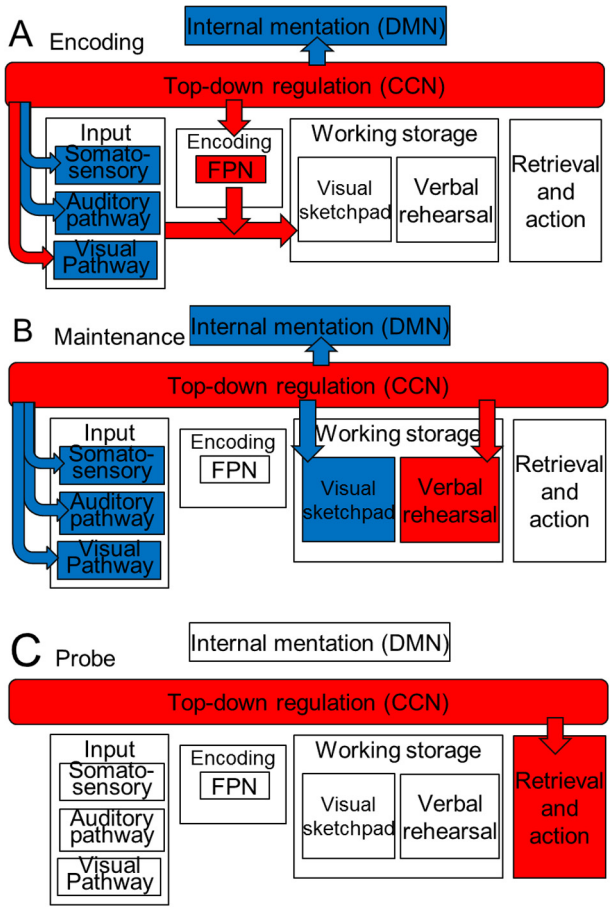

Fig. 5. Schematic summary of the CCN's top-down regulatory function in the current working memory task. Red and blue denote activation and suppression, respectively. Abbreviation: CCN, core control network; DMN, default mode network; FPN, frontoparietal network.

During the maintenance stage, we observed deactivation in the visual cortices, auditory cortices, and S-II, which indicates that most sensory input channels were shut down to prevent external interference (Fig. 5B). Maintenance stage deactivation in some of these regions was negatively correlated with RTs, indicating that external inputs in this stage may disturb the maintenance of task-relevant information and therefore need to be suppressed. The deactivation was stronger under greater load conditions. Furthermore, the deactivation of the visual cortex in maintenance stage is in agreement with our previous finding of alpha power increase in higher load conditions during verbal WM task, indicating decreased excitability to gate out external interference to protect the information held online (Anderson and Ding, 2011; Wang et al., 2016). The suppression of the irrelevant sensory inputs was released in the probe stage (Fig. 5C).

Functional differences between the CCN and FPN

Researchers have reached a consensus that prefrontal regions can exert top-down attentional control and influence which low-level features are selected to be encoded in WM (Altamura et al., 2007; Xu, 2017). But there is an ongoing debate about which system underlies the top-down control during highly demanding tasks such as attention and WM. Some researchers have proposed that the FPN maintains WM and underlies the top-down control to guarantee task focus (Corbetta, et al., 2002). Others have proposed that the CCN provides top-down control (Corbetta, et al., 2008). We observed strong CCN activation in all WM stages but strong FPN activation only in the encoding stage (Fig. 2B). The distinct activation patterns of the 2 networks suggest that their functional roles are different, although both are considered CES candidates that are essential in top-down control (Curtis, 2006; Xu, et al., 2014). The CCN may supervise the entire task, with responsibility for initiating and maintaining WM, monitoring and regulating the slave systems, and terminating or switching the task (Cai, et al., 2016; Dosenbach, et al., 2006; Kolling et al., 2016). The FPN may function on a trial level by initiating and maintaining attention that enhances the processing of task-relevant information (Corbetta, et al., 2008).

Our results may also elucidate long-running questions about the FPN's functional role in WM and attention, as we observed FPN activation in WM and attention tasks. Some researchers have proposed that the FPN is mainly an attention network whose activation in WM reflects the need for attention (Corbetta, et al., 2008; Wen, et al., 2013; Wen et al., 2012), while others have suggested that it is mainly a WM network that temporally stores information. Its activation during attention reflects temporal attention set maintenance in WM (Corbetta, et al., 2008). Our study, which separately examined activation patterns in each WM stage, clearly showed that the FPN was strongly activated only in the encoding stage, which suggests that it may be more important when attention is required to selectively enhance the processing of task-relevant information.

In summary, although people have linked numerous frontal and parietal structures to CES, our results indicate that CCN is the most likely candidate underlying CES which regulates the middle class (including FPN) and the lower class (including the sensory channels) in all WM stages, while FPN mainly regulates the sensory channels in encoding stage.

Buffer system regulation in WM

Our results suggest that 2 cortical systems being related to WM buffer may be regulated according to the task demands (Fig. 5B). We found strong maintenance stage activation of the left IFG and left middle temporal gyrus, which are proposed to form the so-called phonological loop, a network responsible for verbal rehearsal in the current WM task (Aboitiz, et al., 2010; Chein, et al., 2003; Glezer, et al., 2016; Hickok and Poeppel, 2007). However, the primary and higher-order visual pathway areas exhibited maintenance stage deactivation. This selective activation/deactivation pattern is consistent with the hypothesis that the CES recruits slave buffers according to current WM task demands.

Strengths and limitations of the current work

This study used a modified Sternberg paradigm, whole-brain GLM analysis, and ROI-based single-trial estimation to separately analyze brain activation and deactivation patterns in different WM stages, thereby elucidating the functional roles of different task-relevant networks and systems. The paradigm utilized the number of items more than the canonical "7" in the highest load condition to challenge the limit of the subjects and induced significant activation/deactivation of several subsystems in different WM stages. Some of the patterns had seldom been reported in previous WM studies, such as deactivation of visual regions associated with visual inputs and visual sketchpad in maintenance stage, and of somatosensory and auditory pathways in encoding and maintenance stages. Our single-trial estimation also provides a way to examine the timecourse and strength of BOLD activity in different regions under different WM conditions, making it possible to explore the relationship between these regions and behavioral outcomes in the WM task.

However, these approaches fall into the scope of univariate analysis, which is designed for inferring relationships between different regions and networks instead of directly assessing communication between them. Further elucidating network interactions and communication in WM will require more advanced functional connectivity analysis tools and tasks designed for them.

Trial-by-trial correlation analysis between BOLD signals and behavioral performance is often nontrivial due to noise and the nature of single-trial fMRI time series, so the results of correlation analysis between BOLD activity and RTs should be considered carefully. Our results were not corrected for multiple comparisons, and the data were very noisy. Overall network-level correlation analysis provides robustness against noise by averaging results, which makes its results more meaningful than those of single ROI-level correlation results for illustrating the networks' functional significance. Despite our efforts to estimate single-trial responses and correlate them with behavioral performance, many regions exhibited no significant correlations between BOLD responses and behavioral performance. This might arise from noisy fMRI signals or BOLD response saturation. The use of more sophisticated task designs and acquisition techniques in future may improve the analysis.

The current study only considered the young healthy subjects. The overall activation results were consistent with many previous studies using young healthy subjects. For example, the dACC-AI activation (Dosenbach et al., 2006; Wen et al., 2013) and the dorsal frontoparietal activation (Merrikhi et al., 2017; Wu et al., 2018; Xu, 2017), as well as the deactivation of DMN in many high-demanding tasks including WM (Anticevic et al., 2010; Bonnelle et al., 2012; Elton and Wei, 2015). Therefore, the current results may be generalized to young healthy populations performing WM tasks. Although previous studies considering populations in different groups, such younger and older people (Cappell et al., 2010; Clapp et al., 2011; Payer et al., 2006; Stern et al., 2008), also showed results in line with the current study, it is still an open and important question that whether and how the processes develops normally or alters in disease.

Additionally, a further important question is whether there is a gender difference in deploying CES functions between men and women performing WM tasks, especially in a verbal scenario. This could be a future direction that may require recruitment of a larger number of subjects of each gender.

Conclusions

We showed the neurobiological bases for some of the essential components in Baddeley's theoretical model of WM. Our results suggest that a CCN comprising the dACC and AI that exhibits consistent activation in all WM stages may play a central role of in regulating other systems, forming the neural basis of CES in Baddley's model. Our results also elucidate the dynamic configuration of other systems, including different buffers, sensory input channels, external attention systems, and internal default systems, according to WM stage demands.

ACKNOWLEDGMENTS

Funding: This work was supported by the General Program of the National Natural Science Foundation of China [grant number 61571047].

CONFLICTS OF INTEREST

None.

REFERENCES

Aboitiz F, Aboitiz S, García RR (2010) The phonological loop: a key innovation in human evolution. Curr Anthropol 51:S55–S65.

Altamura M, Elvevåg B, Blasi G, Bertolino A, Callicott JH, Weinberger DR, Mattay VS, Goldberg TE (2007) Dissociating the effects of Sternberg working memory demands in prefrontal cortex. Psychiatry Res: Neuroimaging 154:103–114.

Anderson KL, Ding M (2011) Attentional modulation of the somatosensory mu rhythm. Neuroscience 180:165–180.

Anticevic A, Repovs G, Shulman GL, Barch DM (2010) When less is more: TPJ and default network deactivation during encoding predicts working memory performance. Neuroimage 49:2638–2648.

Anticevic A, Repovs G, Barch DM (2013) Working memory encoding and maintenance deficits in schizophrenia: neural evidence for activation and deactivation abnormalities. Schizophr Bull 39:168–178.

Baddeley A (1974) Working memory. Psychol Learn Motivat 8:47–89.

Baddeley A (2000) The episodic buffer: a new component of working memory? Trends Cogn Sci 4:417–423.

Baddeley A (2012) Working memory: theories, models, and controversies. Annu Rev Psychol 63:1–29.

Baddeley A, Wilson BA (2002) Prose recall and amnesia: implications for the structure of working memory. Neuropsychologia 40:1737–1743.

Bonnelle V, Ham TE, Leech R, Kinnunen KM, Mehta MA, Greenwood RJ, Sharp DJ (2012) Salience network integrity predicts default mode network function after traumatic brain injury. PNAS 109:4690–4695.

Bressler SL, Menon V (2010) Large-scale brain networks in cognition: emerging methods and principles. Trends Cogn Sci 14:277–290.
Buckner RL, Andrews-Hanna JR, Schacter DL (2008) The Brain's default Network. Ann N Y Acad Sci 1124:1–38.
Cai W, Chen T, Ryali S, Kochalka J, Li CSR, Menon V (2016) Causal interactions within a frontal-cingulate-parietal network during cognitive control: convergent evidence from a multisite-multitask investigation. Cereb Cortex 26:2140–2153.
Cappell AK, Gmeindl L, Reuter-Lorenz PA (2010) Age differences in prefontal recruitment during verbal working memory maintenance depend on memory load. Cortex 46:462–473.
Chacko A, Bedard AC, Marks DJ, Feirsen N, Uderman JZ, Chimiklis A, Rajwan E, Cornwell M, et al. (2014) A randomized clinical trial of Cogmed Working Memory Training in school-age children with ADHD: a replication in a diverse sample using a control condition. J Child Psychol Psychiatry 55:247–255.
Chein JM, Ravizza SM, Fiez JA (2003) Using neuroimaging to evaluate models of working memory and their implications for language processing. J Neurolinguistics 16:315–339.
Clapp WC, Rubens MT, Sabharwal J, Gazzaley A (2011) Deficit in switching between functional brain networks underlies the impact of multitasking on working memory in older adults. PNAS 108:7212–7217.
Cohen JR, Sreenivasan KK, D'Esposito M (2014) Correspondence between stimulus encoding- and maintenance-related neural processes underlies successful working memory. Cereb Cortex 24:593–599.
Cole MW, Schneider W (2007) The cognitive control network: Integrated cortical regions with dissociable functions. Neuroimage 37:343–360.
Collins DL, Neelin P, Peters TM, Evans AC (1994) Automatic 3D intersubject registration of MR volumetric data in standardized Talairach space. J Comput Assist Tomogr 18:192–205.
Constantinidis C, Klingberg T (2016) The neuroscience of working memory capacity and training. Nat Rev Neurosci 17:438–449.
Corbetta M, Kincade JM, Shulman GL (2002) Neural systems for visual orienting and their relationships to spatial working memory. J Cognit Neurosci 14:508–523.
Corbetta M, Patel G, Shulman GL (2008) The reorienting system of the human brain: from environment to theory of mind. Neuron 58:306–324.
Courtney SM, Ungerleider LG, Keil K, Haxby JV (1997) Transient and sustained activity in a distributed neural system for human working memory. Nature 386:608–611.
Curtis CE (2006) Prefrontal and parietal contributions to spatial working memory. Neuroscience 139:173–180.
D'Esposito M, Detre JA, Alsop DC, Shin RK, Atlas S, Grossman M (1995) The neural basis of the central executive system of working memory. Nature 378:279–281.
D'Esposito M, Postle BR (2015) The cognitive neuroscience of working memory. Annu Rev Psychol 66:115–142.
Dosenbach NUF, Visscher KM, Palmer ED, Miezin FM, Wenger KK, Kang HC, Burgund ED, Grimes AL, et al. (2006) A core system for the implementation of task sets. Neuron 50:799–812.
Dosenbach NUF, Fair DA, Miezin FM, Cohen AL, Wenger KK, Dosenbach RAT, Fox MD, Snyder AZ, et al. (2007) Distinct brain networks for adaptive and stable task control in humans. PNAS 104:11073–11078.
Dovis S, Oord SVD, Wiers RW, Prins PJM (2012) Can motivation normalize working memory and task persistence in children with attention-deficit/hyperactivity disorder? The effects of money and computer-gaming. J Abnorm Child Psychol 40:669–681.
Elton A, Wei G (2015) Task-positive functional connectivity of the default mode network transcends task domain. J Cognit Neurosci 27:2369–2381.
Eriksson J, Vogel EK, Lansner A, Bergström F, Nyberg L (2015) Neurocognitive architecture of working memory. Neuron 88:33–46.
Glezer LS, Eden G, Xiong J, Luetje M, Napoliello E, Kim J, Riesenhuber M (2016) Uncovering phonological and orthographic selectivity across the reading network using fMRI-RA. Neuroimage 138:248–256.
Hanslmayr S, Volberg G, Wimber M, Raabe M, Greenlee MW, Bäuml KH (2012) The relationship between brain oscillations and BOLD signal during memory formation: a combined EEG–fMRI study. J Neurosci 31:15674–15680.
Harding IH, Harrison BJ, Breakspear M, Pantelis C, Yücel M (2016) Cortical representations of cognitive control and working memory are dependent yet non-interacting. Cereb Cortex 26:557.
Hickok G, Poeppel D (2007) The cortical organization of speech processing. Nat Rev Neurosci 8:393–402.
Jilka SR, Scott G, Ham T, Pickering A, Bonnelle V, Braga RM, Leech R, Sharp DJ (2014) Damage to the salience network and interactions with the default mode network. J Neurosci Off J Soc Neurosci 34:10798–10807.
Kofler MJ, Rapport MD, Bolden J, Sarver DE, Raiker JS (2010) ADHD and working memory: the impact of central executive deficits and exceeding storage/rehearsal capacity on observed inattentive behavior. J Abnorm Child Psychol 38:149–161.
Kolling N, Behrens T, Wittmann MK, Rushworth M (2016) Multiple signals in anterior cingulate cortex. Curr Opin Neurobiol 37:36–43.
Leung HC, Seelig D, Gore JC (2004) The effect of memory load on cortical activity in the spatial working memory circuit. Cogn Affect Behav Neurosci 4:553–563.
Logie RH (2003) Spatial and visual working memory: a mental workspace. Psychol Learn Motivat 42:37–78.
Menon V (2015) Salience Network A2 – Toga. In: Arthur W, editor. Brain Mapping. Waltham: Academic Press. p. 597–611.
Menon V, Uddin LQ (2010) Saliency, switching, attention and control: a network model of insula function. Brain Struct Funct 214:655–667.
Merrikhi Y, Clark K, Albarran E, Parsa M, Zirnsak M, Moore T, Noudoost B (2017) Spatial working memory alters the efficacy of input to visual cortex. Nat Commun 8:15041.
Miller EK, Erickson CR (1996) Neural mechanisms of visual working memory in prefrontal cortex of the macaque. J Neurosci 16:5154–5167.
Osaka M, Komori M, Morishita M, Osaka N (2007) Neural bases of focusing attention in working memory: an fMRI study based on group differences. Cogn, Affect, Behav Neurosci 7:130–139.
Osaka N, Osaka M, Kondo H, Morishita M, Fukuyama H, Shibasaki H (2004) The neural basis of executive function in working memory: an fMRI study based on individual differences. Neuroimage 21:623–631.
Payer D, Marshuetz C, Sutton B, Hebrank A, Welsh RC, Park DC (2006) Decreased neural specialization in old adults ona working memory task. NeuroReport 17:487–491.
Pesaran B, Pezaris JS, Sahani M, Mitra PP, Andersen RA (2002) Temporal structure in neuronal activity during working memory in macaque parietal cortex. Nat Neurosci 5:805–811.
Pessoa L, Gutierrez E, Bandettini PA, Ungerleider LG (2002) Neural correlates of visual working memory: fMRI amplitude predicts task performance. Neuron 35:975–987.
Peterburs J, Cheng DT, Desmond JE (2016) The Association between eye movements and cerebellar activation in a verbal working memory task. Cereb Cortex 26:3802–3813.
Piccoli T, Valente G, Linden DE, Re M, Esposito F, Sack AT, Di SF (2015) The default mode network and the working memory network are not anti-correlated during all phases of a working memory task. PLoS ONE 10:1–16.
Redick TS, Shipstead Z, Harrison TL, Hicks KL, Fried DE, Hambrick DZ, Kane MJ, Engle RW (2013) No evidence of intelligence improvement after working memory training: a randomized, placebo-controlled study. J Exp Psychol Gen 142:359–379.
Reed JL, Gallagher NM, Sullivan M, Callicott JH, Green AE (2017) Sex differences in verbal working memory performance emerge at very high loads of common neuroimaging tasks. Brain Cogn 113:56–64.

Rypma B, Prabhakaran V, Desmond JE, Glover GH, Gabrieli JDE (1999) Load-dependent roles of frontal brain regions in the maintenance of working memory. NeuroImage 9:216–226.

Shenhav A, Cohen JD, Botvinick MM (2016) Dorsal anterior cingulate cortex and the value of control. Nat Neurosci 19:1286–1291.

Stern Y, Zarahn E, Habeck C, Holtzer R, Rakitin BC, Kumar A, Flynn J, Steffener J, et al. (2008) A common neural network for cognitive reserve in verbal and object working memory in young but not old. Cereb Cortex 18:959–967.

Stopford CL, Thompson JC, Neary D, Richardson AM, Snowden JS (2012) Working memory, attention, and executive function in Alzheimer's disease and frontotemporal dementia. Cortex 48:429–446.

Wallis G, Stokes M, Cousijn H, Woolrich M, Nobre AC (2015) Frontoparietal and Cingulo-opercular networks play dissociable roles in control of working memory. J Cognit Neurosci 27:2019–2034.

Wang C, Rajagovindan R, Han SM, Ding M (2016) Top-down control of visual alpha oscillations: sources of control signals and their mechanisms of action. Front Hum Neurosci 10:15.

Wen X, Yao L, Liu Y, Ding M (2012) Causal interactions in attention networks predict behavioral performance. J Neurosci 32:1284–1292.

Wen X, Liu Y, Yao L, Ding M (2013) Top-down regulation of default mode activity in spatial visual attention. J Neurosci 33:6444–6453.

Wu Y-h, Uluç I, Schmidt TT, Tertel K, Kirilina E, Blankenburg F (2018) Overlapping frontoparietal networks for tactile and visual parametric working memory representations. NeuroImage 166:325–334.

Xu Y (2017) Reevaluating the sensory account of visual working memory storage. Trends Cogn Sci 21:794–815.

Xu J, Calhoun VD, Pearlson GD, Potenza MN (2014) Opposite modulation of brain functional networks implicated at low vs. high demand of attention and working memory. Plos One 9 e87078.

(Received 3 April 2018, Accepted 4 September 2018)
(Available online 9 September 2018)